Longitudinally propagating traveling waves of the mammalian tectorial membrane

Roozbeh Ghaffari*†, Alexander J. Aranyosi†, and Dennis M. Freeman*†‡§¶

*Speech and Hearing Bioscience and Technology Program, Harvard–MIT Division of Health Sciences and Technology, Cambridge, MA 02139; †Research Laboratory of Electronics and ‡Department of Electrical Engineering and Computer Science, Massachusetts Institute of Technology, Cambridge, MA 02139; and §Eaton–Peabody Laboratory of Auditory Physiology, Massachusetts Eye and Ear Infirmary, Boston, MA 02114

Edited by David P. Corey, Harvard Medical School, Boston, MA, and accepted by the Editorial Board August 27, 2007 (received for review April 23, 2007)

Sound-evoked vibrations transmitted into the mammalian cochlea produce traveling waves that provide the mechanical tuning necessary for spectral decomposition of sound. These traveling waves of motion that have been observed to propagate longitudinally along the basilar membrane (BM) ultimately stimulate the mechano-sensory receptors. The tectorial membrane (TM) plays a key role in this process, but its mechanical function remains unclear. Here we show that the TM supports traveling waves that are an intrinsic feature of its visco-elastic structure. Radial forces applied at audio frequencies (2–20 kHz) to isolated TM segments generate longitudinally propagating waves on the TM with velocities similar to those of the BM traveling wave near its best frequency place. We compute the dynamic shear storage modulus and shear viscosity of the TM from the propagation velocity of the waves and show that segments of the TM from the basal turn are stiffer than apical segments are. Analysis of loading effects of hair bundle stiffness, the limbal attachment of the TM, and viscous damping in the subtectorial space suggests that TM traveling waves can occur *in vivo*. Our results show the presence of a traveling wave mechanism through the TM that can functionally couple a significant longitudinal extent of the cochlea and may interact with the BM wave to greatly enhance cochlear sensitivity and tuning.

cochlear mechanics | dynamic mechanical properties | longitudinal mechanical coupling

The mammalian cochlea is a remarkable sensor that can detect motions smaller than the diameter of a hydrogen atom and can perform high-quality spectral analysis to discriminate as many as 30 frequencies in the interval of a single semitone (1, 2). These extraordinary properties of the hearing organ depend on traveling waves of motion that propagate along the basilar membrane (BM) (3) and ultimately stimulate the mechano-sensory receptors. There are two types of cochlear receptors: the inner and outer hair cells (OHCs). Both types of hair cells contain densely packed arrays of stereocilia called hair bundles that transduce mechanical energy into electrical signals (4). These hair bundles project from the apical surface of hair cells toward an overlying gelatinous matrix called the tectorial membrane (TM).

The strategic anatomical configuration of the TM relative to the hair bundles suggests that the TM plays a key role in stimulating hair cells. Mouse models with genetically modified structural components of the TM have been shown to exhibit severe loss of cochlear sensitivity and altered frequency tuning (5–9), thereby providing further evidence that the TM is required for normal cochlear function. However, the mechanical processes by which traveling wave motion along the BM leads to hair cell stimulation remain unclear (10), largely because the important mechanical properties of the TM have proved difficult to measure. Consequently, the mechanical function of the TM has been variously described as a rigid pivot, a resonant structure, and a free-floating mass (11–14) in "classical" cochlear models, which assume that adjacent longitudinal sections of the cochlea are uncoupled except for energy propagation through the fluid (15). Recent measurements have shown that the TM is visco-elastic (16) and can couple motion over significant longitudinal cochlear distances (9, 16), suggesting that the TM also may support waves. Such waves have been predicted previously in the amphibian inner ear based on neurophysiological evidence (17). Here we show that longitudinally propagating traveling waves are intrinsic to the dynamic material properties of the mammalian TM. The longitudinal extent of wave motion suggests that TM waves can stimulate hair cells from multiple regions of the cochlea and interact with the BM traveling wave to affect cochlear function.

Results and Discussion

To study wave propagation in the TM, we developed an experiment chamber in which a segment of an isolated TM from the mouse cochlea is suspended between two parallel-aligned supports in artificial endolymph (Fig. 1*A*). Sinusoidal forces applied in the radial direction at one support launched waves that propagated longitudinally along the TM toward the other support [Fig. 1*B*; see supporting information (SI) Movie 1]. TM waves were bidirectional; attaching either the basal or apical end of the TM to the vibrating support launched waves. These waves were generated with nanometer-scale amplitudes (≈90–400 nm) over a broad range of frequencies (2–20 kHz). An optical imaging system synchronous with the driving stimulus (18) tracked radial displacement amplitude and phase at multiple points on the surface of the TM (see *Materials and Methods*).

Longitudinal Pattern of TM Radial Motion. Fig. 2*A* shows the spatial pattern of radial displacement of a typical basal TM segment in response to 15-kHz motion of one support. The two waveforms show radial displacement as a function of longitudinal distance at two instants of time separated by 1/4 cycle. An exponentially decaying sinusoid was fit to each waveform. These fits indicate wave motion of the TM. The wave has a wavelength of 350 μm, and the amplitude decays with a space constant of 237 μm. The wavelength did not vary with displacement of the vibrating support. Moreover, radial displacement along the TM scaled linearly with displacement of the support.

Author contributions: R.G., A.J.A., and D.M.F. designed research; R.G. performed research; R.G. and A.J.A. analyzed data; and R.G., A.J.A., and D.M.F. wrote the paper.

The authors declare no conflict of interest.

This article is a PNAS Direct Submission. D.P.C. is a guest editor invited by the Editorial Board.

Freely available online through the PNAS open access option.

Abbreviations: BM, basilar membrane; TM, tectorial membrane; OHC, outer hair cell; BF, best frequency; IHC, inner hair cell.

¶To whom correspondence should be addressed at: Massachusetts Institute of Technology, 77 Massachusetts Avenue, Room 36-889, Cambridge, MA 02139. E-mail: freeman@mit.edu.

This article contains supporting information online at www.pnas.org/cgi/content/full/0703665104/DC1.

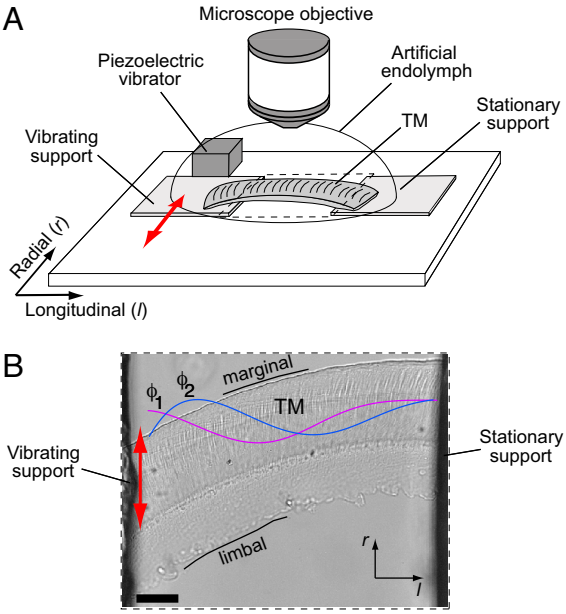

Fig. 1. Suspended TM segment in a wave chamber. (*A*) Schematic of TM segment suspended between two supports (not to scale). Double-headed arrow indicates sinusoidal displacement of vibrating support at audio frequencies. Radial displacement of the TM was tracked at audio frequencies by using stroboscopic illumination (see *Materials and Methods*). (*B*) Image of TM segment taken with a light microscope. (Scale bar, 50 μm.) Displacement and phase of propagating motion were tracked at several points along the TM in the region that normally overlies the hair bundles. Marginal and limbal boundaries of the TM are indicated. The two schematic waveforms pasted on the image are displacement snapshots at sequential instants (ϕ_1, ϕ_2) illustrating typical TM deformations. Displacement amplitudes were exaggerated to show the wave-like nature of the motion.

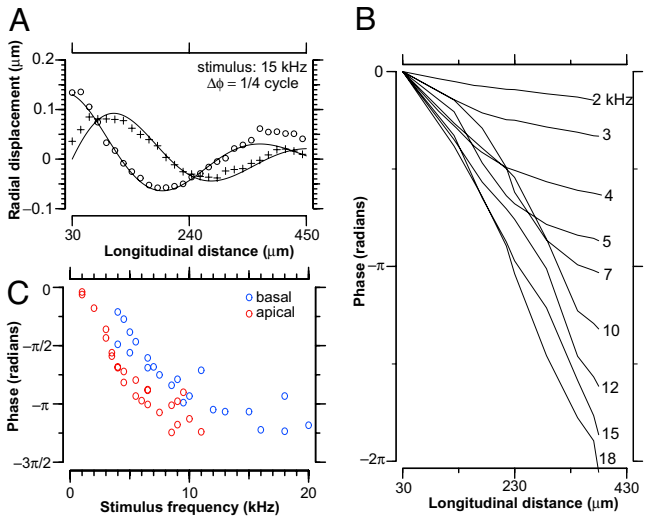

Fig. 2. Traveling waves along isolated TM segments. (*A*) TM radial displacement vs. longitudinal distance in response to 15-kHz stimulation. Radial displacement (r) is plotted as a function of longitudinal distance (x) at two instants separated by 1/4 cycle for a TM segment from the upper basal turn. Solid lines represent the equation $r = 0.13e^{-(x-30)/237}\cos(2\pi(x - 30)/350 - \phi)$, with x and r in micrometers and $\phi = 0$, $\pi/2$ radians. Longitudinal distance was measured relative to a point on the TM $\approx$30 μm from the edge of vibrating support. (*B*) Phase vs. longitudinal distance for stimulus frequencies 2–18 kHz of the basal TM segment from *A*. Phase is plotted relative to a 30-μm point on the TM. Phases decreased monotonically with distance and became steeper with increasing frequency. (*C*) Phase vs. stimulus frequency at a location on the surface of the TM $\approx$250 μm from vibrating support. Each symbol represents phase lag measured relative to a 30-μm point on the TM. Apical TMs (red; n = 25 measurements) accumulated more phase lag than basal TMs (blue; n = 22 measurements) at a given stimulus frequency. The entire data set represents measurements across six TM preparations (three basal and three apical TMs).

The phase of radial displacement varied with longitudinal distance in a frequency-dependent manner. In Fig. 2*B*, the phase lag at low frequencies (2 kHz) reached $\pi/6$ radians over the length of the suspended TM. In contrast, at high frequencies ($\geq$18 kHz), the phase lag exceeded a complete cycle ($>2\pi$ radians). Phase also was measured as a function of stimulus frequency at a location on the surface of the TM $\approx$250 μm from the vibrating support. Fig. 2*C* shows that phase lag increased with stimulus frequency. This trend was evident across all TM samples, and the lag was larger for TM segments from the apical turn of the cochlea than for segments from the basal turn.

Waves Intrinsic to Dynamic Material Properties of the TM. The velocity of wave propagation (v_s) was computed as the product of frequency and wavelength for each stimulus frequency. For pure shear waves in an infinite, isotropic, visco-elastic material, v_s is related to the shear storage modulus (G') and the shear viscosity (η), by

$$v_s = \sqrt{\frac{2(G'^2 + \omega^2\eta^2)}{\rho(G' + \sqrt{G'^2 + \omega^2\eta^2})}}, \qquad [1]$$

where ω is the angular frequency of vibration and ρ is the density of the material (19), assumed to equal that of water. Thus we can estimate G' and η by finding those values for which Eq. **1** best fits measurements of the frequency dependence of v_s. This relationship highlights the material properties that give rise to TM waves. At low frequencies, the wave velocity is determined by the ratio of G' to ρ. At high frequencies, the relevant ratio is $\omega\eta/\rho$. Thus the density, shear modulus, and shear viscosity all contribute to wave propagation.

Distributed Impedance Model of the TM. Although the isolated TM can support waves, the TM is loaded *in vivo* by hair bundles and damped by fluid in the subtectorial space (12, 13). To test the effects of these loads, we analyzed a distributed impedance model of the TM. The model consisted of a longitudinally distributed series of masses (M) coupled by viscous (b) and elastic (k) elements (Fig. 3*A*). The radial displacements of the TM at the supports were constrained in the model as they were in the wave chamber. Moreover, in contrast to Eq. **1**, this model accounts for the finite dimensions of the TM. The value for each mass component was determined by assuming the TM had the density of water. The k and b parameters are related to the shear storage modulus and shear viscosity of the TM by $G' = kd/A_{TM}$ and $\eta = bd/A_{TM}$, where d is the length of each longitudinal section and A_{TM} is the cross-sectional area. Sinusoidal stimuli applied to one end of the TM in this model launched a traveling wave similar to those seen in the wave chamber. The model accounts for the fact that fluid adjacent to the TM moves with the TM in a frequency-dependent fluid boundary layer. Fluid velocity in this layer can be approximated by

$$U(y, \omega) = U_{TM}e^{-y\sqrt{j\omega\rho/\mu}}, \qquad [2]$$

where ω is the radial frequency, U_{TM} is the velocity of the TM, y is the height above the TM, and ρ and μ are fluid density and viscosity, respectively (20). This fluid layer significantly increases the effective mass of the TM and causes some damping (b_{bl}). The best fit of the model to the measurements of a typical TM segment from the upper basal turn is shown in Fig. 3*B*.

Estimates of TM material properties from the distributed impedance model vary with longitudinal cochlear position. The

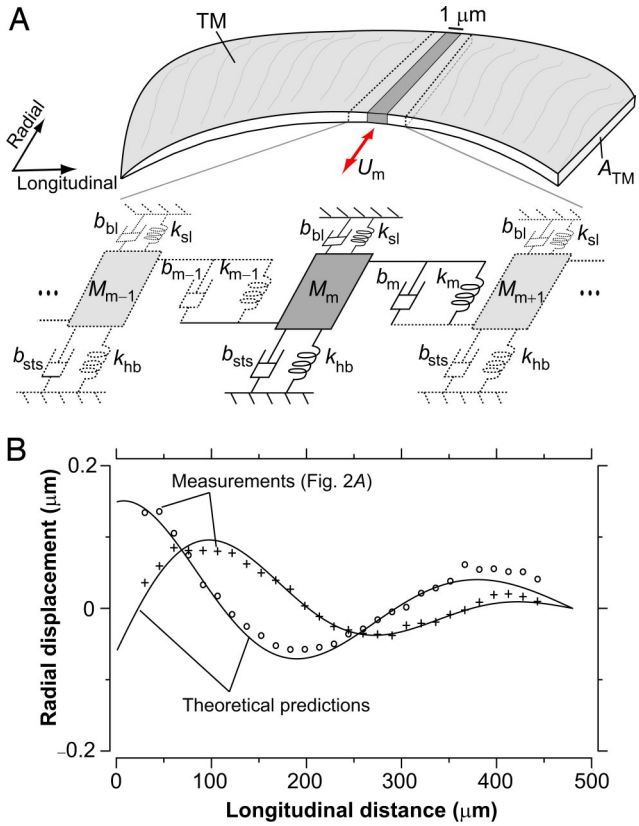

Fig. 3. Distributed impedance model of the TM. (*A*) (*Upper*) Schematic highlighting a 1-μm longitudinal section (*d*) of the TM (dark gray) with rectangular cross-sectional area, A_{TM}. Vibrating support can generate radial motion of this TM section with a velocity of U_m through longitudinal coupling. (*Lower*) Mechanical circuit representation of TM section consisting of a mass (M_m) coupled to adjacent sections (M_{m-1}, M_{m+1}) by viscous (b_m, b_{m-1}) and elastic (k_m, k_{m-1}) components. The effective mass of each TM section included the mass of the fluid layers above and below the TM. Effect of damping in the fluid layer was investigated by adding a dashpot (b_{bl}) between each mass and ground. Effects of cochlear loads: viscous damping in the subtectorial space (b_{sts}), hair bundle stiffness (k_{hb}), and the elastic effect of the limbal attachment (k_{sl}) were investigated by adding a dashpot and two springs between each mass and ground. (*B*) Comparison of TM wave measurements in the wave chamber to theoretical predictions of the distributed impedance model. Symbols (+ and ○) denote motion measurements of the upper basal TM segment from Fig. 2*A*. Lines represent least-squares fits of the theoretical predictions to these experimental results. The best fit values of shear storage modulus, G', and shear viscosity, η, applied in the model across multiple frequencies for this TM were 30 kPa and 0.13 Pa·s, respectively. Velocities at the extreme longitudinal ends of the TM segment were constrained in the model as they were by the supports in the TM wave experiments.

mean values of the shear storage modulus, G', for basal and apical TM segments were 47 ± 12 kPa (n = 5 TM preparations) and 17 ± 5 kPa (n = 3 TM preparations), respectively. The ranges denote the standard deviation from the mean. The greater G' values of basal TMs indicate that portions of the TM from the basal turn are stiffer than those from the apical turn, as has been reported by others (21–23). Moreover, the range of G' values in the present study is somewhat larger than previous estimates of this property (21, 23, 24) with one important exception. Gueta *et al.*'s (22) quasi-static measurements in the base of the mouse cochlea are significantly larger than any other reported values. It is difficult to make comparisons of G' across studies because the TM is anisotropic (16) and the methods are different: we provide a radial stimulus that generates shear waves, whereas others (22–24) analyze transverse point indentations. Furthermore, these previous measurements were made at static or near static (1–10 Hz) conditions (21–24), and the mechanical properties of the TM vary with frequency (16). Thus a meaningful comparison with previous measurements requires development of a theoretical framework for comparing quasi-static and audio-frequency results. The mean values of TM shear viscosity, η, ranged from 0.11 to 0.26 Pa·s, which is much greater than the viscosity of water (0.001 Pa·s). These large values of shear viscosity could result because the porous network of TM macromolecules resists the flow of interstitial fluid or because of proteoglycan interactions. Although the mean values of η were greater in basal TM segments (0.19 ± 0.07 Pa·s) than in apical segments (0.15 ± 0.04 Pa·s), the large ranges preclude any strong conclusions about longitudinal trends.

To predict the effects of hair bundle stiffness and viscous damping in the subtectorial space, a spring (k_{hb}) representing hair bundles and a dashpot (b_{sts}) representing fluid damping were added between each mass and ground (Fig. 3*A*). We assumed that a nominal hair bundle stiffness of 3.5 mN/m (25) was distributed evenly across an 8-μm extent of the TM for each of the three rows of OHCs. Adding hair bundle stiffness to the model increased space constants by ≈1%. Damping in the subtectorial space, b_{sts}, was estimated assuming that fluid flow was Couette, so that

$$b_{sts} = \frac{\mu A_{sts}}{\delta}, \qquad [3]$$

where μ is the viscosity of the fluid in the space and A_{sts} is the cross-sectional area of each TM section facing the subtectorial space. The height of the subtectorial space, δ, was taken to be 1–6 μm based on the lengths of OHC stereocilia (26). Although the TM has a large intrinsic damping, viscous damping in the subtectorial space still has some frequency-dependent effects on wave motion at the narrowest gaps (δ = 1 μm). In response to 7-kHz stimuli, the space constants of wave motion of a typical basal TM decreased by ≈50%. At 10 kHz, the space constants were reduced by ≈25%. These reductions in the space constants were evident only for δ = 1 μm and insignificant for $\delta > 2$ μm. This finding suggests that subtectorial damping would have a significant effect on TM wave propagation at low frequencies only for the narrowest gaps, which occur in the extreme base of the cochlea (26). Because the base of the cochlea responds to high frequencies, damping in the subtectorial space does not significantly affect wave propagation near the best frequencies (BFs) of basal cochlear locations.

An additional effect of including the subtectorial space in the model was to reduce the effective mass of the TM, because the subtectorial space replaced the lower fluid boundary layer. This reduction in mass caused an increase in wavelengths particularly at low frequencies. In response to 7-kHz and 10-kHz stimuli, the wavelengths were increased by ≈15% and ≈10%, respectively. Therefore, replacing the lower boundary layer with the subtectorial space increased wavelengths because of the reduced effective mass of the TM.

There is little agreement on the mechanical properties of the thin attachment of the TM to the spiral limbus. Models of this region of the TM have ranged from completely rigid to mechanically inconsequential (16). Although there is a lack of experimental evidence to support either claim, evidence of TM radial motion in the intact cochlea (27) suggests that the limbal attachment does not preclude TM waves. We analyzed the effects of an elastic limbal attachment by adding a spring (k_{sl}) between each mass and ground (Fig. 3*A*). For sufficiently large values of k_{sl}, the limbal attachment increased the space constant and wavelength of the TM wave at low and intermediate frequencies. The model ultimately demonstrates that TM inertia, damping, and elasticity, which are comparable to those of the

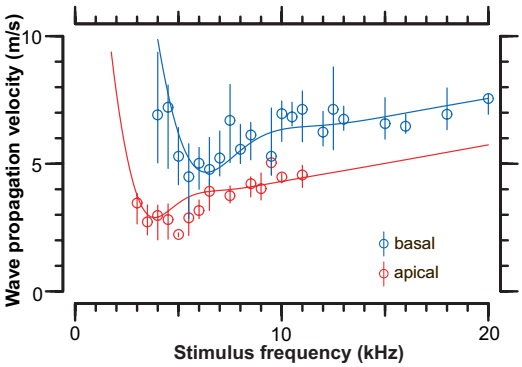

Fig. 4. Propagation velocity of TM traveling waves. The circles represent the median values of wave propagation velocity, ν_s, measured across multiple frequencies for basal (blue; $n = 7$ TM preparations) and apical (red; $n = 4$ TM preparations) segments. Interquartile ranges are represented with vertical lines. Lines represent model predictions of ν_s vs. frequency generated from the average dimensions of basal and apical TM segments and from material property estimates (G' and η) of these segments. Typical values of G' and η for basal ($G' = 40$ kPa; $\eta = 0.33$ Pa·s) and apical ($G' = 16$ kPa; $\eta = 0.18$ Pa·s) TM segments were applied to estimate the frequency dependence of ν_s in the model.

entire cochlear partition (28, 29), allow TM waves to propagate even in the presence of the loads imposed by fluid in the subtectorial space, the hair bundles, and the limbal attachment.

Frequency Dependence of Wave Propagation Velocity. The average dimensions and typical values of G' and η for basal ($G' = 40$ kPa; $\eta = 0.33$ Pa·s) and apical ($G' = 16$ kPa; $\eta = 0.18$ Pa·s) TMs were applied in the model to compute the frequency dependence of wave propagation velocity, ν_s. The measurements of ν_s across basal ($n = 7$ TM preparations) and apical ($n = 4$ TM preparations) TMs were fit by the model predictions (Fig. 4). The model curves and measurements have two distinct regions at low frequencies, an asymptote to infinity and a local minimum, that were dominated by the effects of the stationary support rather than by the material properties of the TM. At frequencies <6 kHz for basal TMs and <4 kHz for apical TMs, the wavelengths of TM waves were significantly greater than the distance between the supports. Consequently, the phase lag at low frequencies approached zero, which in turn caused ν_s to increase asymptotically to larger values (Fig. 4). The local minima were likely caused by wave reflections about the stationary support. Wave reflections can interfere with forward propagating waves and thereby reduce the effective wave propagation velocity in the forward direction. We tested these features by increasing the distance between the boundaries in the model. This change in distance shifted the asymptotes and minima to lower frequencies, consistent with the concept that the stationary boundary increases ν_s and generates wave reflections at low frequencies.

Wave Propagation Not Driven by Fluid Motion. Because the vibrating support drives the surrounding fluid as well as the TM in the wave chamber, we must consider the possibility that the TM is entrained to the fluid, and the observed waves are in fact fluid waves. Fluid motion decreases with increasing distance from the vibrating support, and the space constant for this decrease is the boundary layer thickness. In a two-dimensional approximation of this experimental setup (i.e., fluid velocity does not vary in the direction orthogonal to the plane of focus), the boundary layer thickness is on the order of 10 μm at 15 kHz (30). This distance is small compared with the space constant of TM wave motion ($\approx$240 μm) measured at 15 kHz, and energy dissipation in the third dimension will make it even smaller. Therefore, the contribution of fluid coupling to TM traveling waves is negligible compared with the effect of the intrinsic properties of the TM.

Longitudinal Spread of Excitation via TM Traveling Waves. The waves reported in this study suggest that significant longitudinal spread of excitation occurs via the TM (9, 31). The distributed impedance model (Fig. 3) provides support for this claim by showing that TM waves are robust enough to overcome viscous dissipation in the subtectorial fluid and are sufficient to excite motions of the hair bundles. TM waves therefore provide a mechanism for extensive longitudinal coupling through cochlear structures. This finding counters a fundamental assumption made in classical cochlear models: that adjacent longitudinal sections of the cochlea are uncoupled (15, 32, 33). The space constant measurements at 15 kHz (Fig. 2*A*) indicate that TM wave motion extends $>$240 μm in the longitudinal direction. This value is much larger than previous estimates from TMs completely attached on one surface to a glass slide (16), suggesting that the attachment conditions in the previous studies significantly reduced space constants. The large spatial extent of TM wave motion is sufficient to stimulate as many as 30 rows of hair bundles, thereby coupling the activity of hair cells from multiple regions of the cochlea.

Effect of OHC Motility Mechanisms on TM Waves. Although we have described TM traveling waves as stimulating hair cells, it is equally plausible that these waves can arise from electromotility of OHCs (25, 34–38). Jia *et al.* recently reported that OHC motility generates radial motion of the TM in the hemicochlea (36, 37). This finding suggests that force generation by multiple rows of OHCs via somatic motility or hair bundle motility may well be the natural driving force along the radial direction that excites longitudinally propagating waves of the TM. The physical attachment of the undersurface of the TM to the OHC hair bundles (26) provides further support that OHC motility can generate radial motion of the TM at multiple points along its surface, in a manner that is similar to how waves were launched in the wave chamber (Fig. 1). In contrast to the OHC hair bundles, the inner hair cell (IHC) hair bundles are not in direct contact with the TM but are coupled to the TM through viscous forces from the subtectorial fluid. Recent measurements using electrical stimulation across isolated turns of the guinea pig cochlea indicate that OHC motility drives radial motion of fluid in the subtectorial space (39). This fluid flow is thought to stimulate the IHC hair bundles at frequencies below 3 kHz. Because OHC motility also drives radial motion of the TM (36, 37), TM waves are likely to provide the coupling that allows OHC motility to enhance the mechanical input to IHCs (8, 36, 37, 39, 40).

Implications for Cochlear Mechanics. The fact that TM traveling waves occur *in vitro* is not surprising considering that waves can be excited in a variety of elastic biological tissues (41). What is striking is that TM traveling waves have large space constants and propagate with velocities (2–10 m/s) (Fig. 4) that are comparable to the BM traveling wave near the BF location in response to BF stimuli (42). Therefore, the velocities of these two independent wave mechanisms can be matched near the BF location and are likely to be coupled through the OHCs, which exhibit active movements in the radial and transverse cochlear directions (25, 34–38). This type of interaction suggests that radial motion of the TM wave excites the OHC hair bundles and drives their active mechanism, which can amplify transverse motion of the BM wave. The contribution of TM waves to amplification is expected to be significant only in the region where the two waves have comparable velocities and are likely to be out of phase with respect to each other. The spatial extent of this region is likely to correspond to frequencies within

approximately an octave of the BF (43). The concept that the mammalian cochlea supports two traveling waves with similar propagation velocities over a limited spatial region has been suggested in a previous cochlear model (44), where the combination of the two waves was shown to produce sharp tuning and emissions.

Relation to TM Resonance. The fact that the TM and BM waves have similar velocities and wavelengths has important implications for the concept of TM resonance (12, 13). Previous measurements of TM and BM relative vibrations in the guinea pig cochlea have supported the idea that the TM and hair bundles behave as a resonant system (27). This type of resonance is believed to arise from the mass of the TM and the compliance of the OHC hair bundles at frequencies 0.5 octave below the characteristic frequency of the BM (13, 27). However, the effects of the TM are analyzed based on the concept of point impedance and are supported by point measurements, both of which ignore longitudinal coupling. Our measurements demonstrate that longitudinal coupling through the TM cannot be ignored and suggest that the phenomenon of TM resonance could be interpreted as a single-point simplification of a propagating TM wave.

Conclusions

We have demonstrated that radial displacements of an isolated TM excite waves of motion that propagate longitudinally with velocities similar to those of the BM traveling wave. Analysis of physiological loading effects of the hair bundles, the limbal attachment of the TM, and fluid viscosity in the subtectorial space suggests that TM waves also can propagate *in vivo*. Because these waves can stimulate hair cells and interact with the BM traveling wave, they constitute a distinct mode of motion (10, 45) that can have a significant effect on cochlear tuning and sensitivity, thereby fundamentally changing the way we think about cochlear mechanisms.

Materials and Methods

Isolated TM Preparation. TM segments were excised from the cochleae of adult male mice (strain B6129F1, 4–10 weeks old; Taconic, Hudson, NY) by using a previously published surgical technique (46). Additionally, TM segments were excised from the CD-1 strain of mice (4–8 weeks old; Taconic). No significant differences were found in the wave properties of TM segments excised from these two strains. In total, five B6129F1 TM segments ($n = 3$ basal and $n = 2$ apical) and six CD-1 TM segments ($n = 4$ basal and $n = 2$ apical) were studied.

The cochlea was surgically removed and placed in an artificial endolymph bath containing 174 mM KCl, 5 mM Hepes, 3 mM dextrose, 2 mM NaCl, and 0.02 mM $CaCl_2$. The bath was equilibrated at pH 7.3 at room temperature. The bone casing of the cochlea was gently chipped away with a #11 scalpel blade until the organ of Corti was exposed. A combination of bright- and dark-field illumination provided visual access to the TM above the organ of Corti with a dissection microscope (Zeiss). A sterilized eyelash was used to remove Reissner's membrane and to lift the TM from the cochlea. TM segments (typically 0.5–1 mm in longitudinal length) were isolated from the organ and placed in a fresh artificial endolymph bath in preparation for experiments in the wave chamber. Segments were classified as basal and apical based on the cochlear turn from which they were excised. As a secondary classification measure, we also measured the distance from the edge of the marginal band to the ridge associated with the attachment of the TM to the spiral limbus (46, 47). The care and use of animals in this study were approved by the Massachusetts Institute of Technology Committee on Animal Care.

Wave Chamber. The wave chamber (Fig. 1) consisted of two parallel supports separated by 390–480 μm. One support was attached with epoxy to a piezo-electric actuator (resonance frequency 138 kHz; Thorlabs Inc., Newton, NJ) and loosely coupled to the underlying glass slide. To minimize transverse motion of the actuator, the surface of the support in contact with the glass slide near the actuator was coated with a thin layer of petroleum jelly (Vaseline) in a region that was dry and isolated from fluid contact. Motion of the actuator loaded with the support and fluid was examined to ensure uniform sinusoidal motion in the radial direction. The frequency response of the vibrating system was characterized over a broad range of frequencies (1–40 kHz). The motion amplitude of the support decreased by ≈6 dB between 1 and 20 kHz and exhibited a resonance at ≈30 kHz. TM radial displacement scaled linearly with motion of the vibrating support over the range of amplitudes (≈90–400 nm) applied to the TM.

The second support was firmly attached to the underlying glass slide. To position a TM segment in this experiment chamber, the surfaces of both supports were coated with 0.3 μl of tissue adhesive (Cell Tak; Collaborative Research, Bedford, MA). The tissue adhesive was dried and rinsed with ethanol resulting in a monolayer of adhesive. Artificial endolymph solution was perfused in the region of the supports and over the adhesive.

The TM segment was injected into this medium with a glass-tip micropipet and suspended between the supports with a sterilized eyelash probe. The motion of the vibrating system was not affected by the attachment of the TM. The suspended region of the TM was ≈200–300 μm above the surface of the underlying glass slide. Once the TM was successfully suspended, it was inspected for curvature. Optical sections were acquired at 0.5-μm intervals through the thickness of the TM by using a light microscope coupled to a piezo-positioner (P-721 PIFOC; Physik Instrumente, Karlsruhe/Palmbach, Germany). The captured images rendered a three-dimensional profile of the TM and indicated a curvature of $<2°$ (<6 μm) at the midpoint between the supports. TM segments also were inspected for structural damage. Segments containing tears or structural abnormalities were discarded.

Motion Analysis with Optical System. The optical system consisted of a ×20 water immersion objective (Zeiss Axioplan) with a 0.5 N.A. and a transmitted light condenser (0.8 N.A.). Images were collected with a 12-bit, 1,024 × 1,024 pixel CCD camera (CAD7–1024A; Dalsa Inc., Waterloo, ON, Canada) by strobing the light-emitting diode (LED). The TM segment was illuminated at 16 evenly spaced stimulus phases over several stimulus cycles. The collected images were analyzed to determine the first eight harmonics of the periodic motion. We computed the magnitude and phase of radial displacement from the series of collected images by using previously published motion-tracking algorithms (18, 48). Radial displacement and phase were measured at multiple points along the suspended surface of the TM segment. The phase lag was measured relative to the phase at a point on the TM ≈ 30 μm from the edge of the vibrating support. The experimental setup was supported by a pneumatic vibration-isolation table that damps ambient vibrations of the surroundings. Displacements at the stationary support were used to evaluate the amount of ambient noise and motion error in the measurement system. The noise floor of the measurement system was ≈15 nm.

We thank C. Shera, J. J. Guinan, A. J. Grodzinsky, and the members of the Cochlear Micromechanics group for helpful discussions and comments on the manuscript. We thank C. Liu and W. T. Freeman for their motion magnification algorithms. This research was supported by National Institutes of Health Grant R01-DC00238. R.G. was supported by a training grant from the National Institutes of Health to the Speech and Hearing Bioscience and Technology Program in the Harvard–MIT Division of Health Sciences and Technology.

1. Kössl M, Russell IJ (1995) *Proc Natl Acad Sci USA* 92:276–279.
2. Dallos P (1996) in *The Cochlea*, eds Dallos P, Popper AN, Fay RR (Springer, New York), pp 1–43.
3. von Békésy G (1960) *Experiments in Hearing* (McGraw–Hill, New York).
4. Hudspeth AJ (1985) *Science* 230:745–752.
5. McGuirt WT, Prasad SD, Griffith AJ, Kunst H, Green GE, Shpargel KB, Runge C, Huybrechts C, Mueller RF, Lynch E *et al.* (1999) *Nat Genet* 23:413–419.
6. Legan PK, Lukashkina VA, Goodyear RJ, Kössl M, Russell IJ, Richardson GP (2000) *Neuron* 28:273–285.
7. Simmler MC, Cohen-Salmon M, El-Amraoui A, Guillaud L, Benichou JC, Petit C, Panthier JJ (2000) *Nat Genet* 24:139–143.
8. Legan PK, Lukashkina VA, Goodyear RJ, Lukashkin AN, Verhoeven K, Camp GV, Russell IJ, Richardson GP (2005) *Nat Neurosci* 8:1035–1042.
9. Russell IJ, Legan PK, Lukashkina VA, Lukashkin AN, Goodyear RJ, Richardson GP (2007) *Nat Neurosci* 10:215–223.
10. Guinan JJ, Jr, Lin T, Cheng H (2005) *J Acoust Soc Am* 118:2421–2433.
11. Davis H (1958) *Ann Otol Rhinol Laryngol* 67:789–801.
12. Allen JB (1980) *J Acoust Soc Am* 68:1660–1670.
13. Zwislocki JJ (1980) *Hear Res* 2:171–182.
14. Mammano F, Nobili R (1993) *J Acoust Soc Am* 93:3320–3332.
15. de Boer E (1997) *J Acoust Soc Am* 101:2148–2150.
16. Abnet CC, Freeman DM (2000) *Hear Res* 144:29–46.
17. Hillery CM, Narins PM (1984) *Science* 225:1037–1039.
18. Aranyosi AJ, Freeman DM (2004) *Biophys J* 87:3536–3546.
19. Chen S, Fatemi M, Greenleaf JF (2004) *J Acoust Soc Am* 115:2781–2785.
20. Freeman DM, Weiss TF (1990) *Hear Res* 48:1–15.
21. Masaki K, Weiss TF, Freeman DM (2006) *Biophys J* 91:2356–2370.
22. Gueta R, Barlam D, Shneck RZ, Rousso I (2006) *Proc Natl Acad Sci USA* 103:14790–14795.
23. Richter CP, Emadi G, Getnick G, Quesnel A, Dallos P (2007) *Biophys J* 93:2265–2276.
24. Shoelson B, Dimitriadis EK, Cai H, Kachar B, Chadwick RS (2004) *Biophys J* 87:2768–2777.
25. Kennedy HJ, Crawford AC, Fettiplace R (2005) *Nature* 433:880–883.
26. Lim DJ (1980) *J Acoust Soc Am* 67:1686–1695.
27. Gummer AW, Hemmert W, Zenner HP (1996) *Proc Natl Acad Sci USA* 93:8727–8732.
28. Freeman DM, Abnet CC, Hemmert W, Tsai BS, Weiss TF (2003) *Hear Res* 180:1–10.
29. Chan DK, Hudspeth AJ (2005) *Biophys J* 89:4382–4395.
30. Freeman DM, Weiss TF (1985) in *Peripheral Auditory Mechanisms*, eds Allen JB, Hall JL, Hubbard A, Neely ST, Tubis A (Springer, Berlin), pp 147–154.
31. Zwislocki JJ, Kletsky EJ (1979) *Science* 204:639–641.
32. Patuzzi R (1996) in *The Cochlea*, eds Dallos P, Popper AN, Fay RR (Springer, New York), pp 186–257.
33. de Boer E (1996) in *The Cochlea*, eds Dallos P, Popper AN, Fay RR (Springer, New York), pp 258–317.
34. Brownell WE, Bader CR, Bertrand D, de Ribaupierre Y (1985) *Science* 227:194–196.
35. Chan DK, Hudspeth AJ (2005) *Nat Neurosci* 8:149–155.
36. Jia S, He DZZ (2005) *Nat Neurosci* 8:1028–1034.
37. Jia S, Zuo J, Dallos P, He DZZ (2005) in *Auditory Mechanisms*, eds Nuttall AL, Ren T, Gillespie P, Grosh K, de Boer E (World Scientific, Singapore), pp 261–269.
38. Kennedy HJ, Evans MG, Crawford AC, Fettiplace R (2006) *J Neurosci* 26:2757–2766.
39. Nowotny M, Gummer AW (2006) *Proc Natl Acad Sci USA* 103:2120–2125.
40. Fridberger A, Tomo I, Ulfendahl M, Boutet de Monvel J (2006) *Proc Natl Acad Sci USA* 103:1918–1923.
41. Greenleaf JF, Fatemi M, Insana M (2003) *Annu Rev Biomed Eng* 91:57–78.
42. Robles L, Ruggero MA (2001) *Physiol Rev* 81:1305–1352.
43. Rhode WS, Recio A (2000) *J Acoust Soc Am* 107:3317–3332.
44. Hubbard A (1993) *Science* 259:68–71.
45. Mountain DC, Cody AR (1999) *Hear Res* 132:1–14.
46. Shah DM, Freeman DM, Weiss TF (1995) *Hear Res* 87:187–207.
47. Keiler S, Richter CP (2001) *Hear Res* 162:91–104.
48. Davis CQ, Freeman DM (1998) *Opt Eng* 37:1299–1304.